High power UV pulsed laser with LMA tapered fiber

V. Roy, L. Desbiens, M. Deladurantaye, Y. Taillon

V. Roy, L. Desbiens, M. Deladurantaye, Y. Taillon, "High power UV pulsed laser with LMA tapered fiber," Proc. SPIE 11260, Fiber Lasers XVII: Technology and Systems, 112601W (21 February 2020); doi: 10.1117/12.2543807

SPIE.

Event: SPIE LASE, 2020, San Francisco, California, United States

High power UV pulsed laser with LMA tapered fiber

V. Roy*, L. Desbiens, M. Deladurantaye, Y. Taillon
INO, 2740 Einstein, Québec, QC, GIP 4S4 Canada

ABSTRACT

A short-pulse Yb-doped fiber laser is reported to yield more than 50 W of UV light after single-pass second- and third-harmonic generation using LBO crystals. The NIR laser generates ns-mJ pulses with average power exceeding 200 W after multipart fiber amplifier stages. The polarization-maintaining LMA tapered fiber used as the last amplifier stage features near diffraction-limited output, narrow linewidth and high polarization extinction ratio. Conversion efficiency from NIR to UV is found near 30%, with output pulse energy as high as 260 μJ for an oscillator pulse repetition frequency of 200 kHz. Generated UV light is seen close to diffraction limit, with M^2 factor measured < 1.3 both along and perpendicular to walk-off axis.

Keywords: Fiber amplifier, Large mode area, Ytterbium, Taper, Frequency conversion, Harmonics generation, LBO crystal.

1. INTRODUCTION

UV harmonic generation requires near-infrared pulsed lasers to have high brightness for efficient conversion, i.e. with simultaneous diffraction limited output and narrow emission linewidth. Solid-state lasers have historically outperformed fiber lasers with greater output power and pulse energy after nonlinear frequency conversion [1]. The relatively tight spectral acceptance of birefringent phase-matching with most nonlinear optical crystals puts a stringent limit to spectral broadening taking place in successive amplifier stages due to self-phase modulation. Nonetheless, tremendous powers were reported in recent years from fiber lasers after single-pass SHG/THG process [2], with the latter taking advantage of high-power quasi-CW laser operation. Such regime yields comparatively low pulse energy and peak power given the relatively high pulse repetition frequency and duty cycle. Largest pulse energies achieved so far from fiber lasers after single-pass SHG/THG were obtained using rod-type fibers in master oscillator and power amplifier systems [3] and coherent beam combining [4]. The poor thermal performances of rod-type fibers, due in part to their peculiar waveguide geometry, makes the latter not particularly suited for very high-power amplifiers.

Tapered fibers have emerged as a distinct approach in recent years, where scaling to large mode areas naturally occurs along the length of the fiber, often starting as single-mode at launching end [5]. The latter offers several advantages over conventional LMA fibers. First and foremost, adiabatic transition of the fundamental mode between the smaller and larger ends of the fiber is expected to yield near diffraction-limited output at the latter. In addition, non-reciprocal propagation of light waves in the cladding along the fiber is known to enhance pump absorption, thus allowing for shorter amplifier fiber. Besides, counter pumping yields B-integrals localized at the very end of the taper, i.e. where the mode field area is the largest. Also, unlike complex fiber designs, conventional step-index profile makes the fiber less sensitive upon fabrication process and packaging constraints.

Here we report on the use of an Yb-doped large mode area tapered fiber as a power amplifier, where seed pulses from a master oscillator are boosted to the mJ level while avoiding deleterious nonlinear effects, which in turn allows for high power UV harmonic generation after single-pass SHG/THG using LBO crystals. Peak power in the 100s kW range after the power amplifier is shown to yield decent efficiency after SHG/THG stage despite relatively loose focusing of NIR beam, with walk-off considered inconsequential. As a result, less burden is put on the conversion stage design, making complex schemes like walk-off compensated crystal stacks or non-axisymmetric optical systems unnecessary, and yet with near diffraction-limited, non-astigmatic and non-elliptical beam readily possible. In the following, a brief outline of the LMA tapered fiber properties and its performances as a laser amplifier are described in section 2. A detailed account of SHG and THG process for UV generation is given in section 3, with the latter to be followed by concluding remarks.

* vincent.roy@ino.ca / www.ino.ca

Fiber Lasers XVII: Technology and Systems, edited by Liang Dong, Proc. of SPIE Vol. 11260, 112601W
 · doi: 10.1117/12.2543807

2. NIR MOPA LASER

2.1 LMA tapered fiber

A large mode area fiber was pulled as a taper from draw tower, starting off from a glass preform fabricated from conventional MCVD and solution doping process. Silica glass composition, with proportions of phosphorous and aluminum oxides near the $AlPO_4$ join [6], was chosen to allow for high concentration Yb doping at the same time as minimizing photodarkening losses. The fiber features core/cladding diameters of 35/250 and 56/400 µm, respectively, at the small and large ends of the flared section. The core NA of 0.065 yields an effective mode area close to 1000 μm^2 according to calculations based on the actual refractive index profile using a mode solver. Suppression of higher-order modes is readily enforced due to the multi-cladding design which features a depressed-index inner cladding layer, with enhanced bending losses for all but the fundamental mode. In addition, confinement of Yb dopants at the core center serves the same purpose, instead this time the higher-order modes are deprived from amplification at the core outer edge where unsaturated gain lies. Both schemes are believed to be effective mitigating strategies to inhibit transverse mode instabilities often seen in high-power fiber amplifiers under large heat loads. Before fiber drawing, the fiber preform was drilled to have boron-doped stress rods inserted as a Panda-type birefringent fiber. Besides, the linear polarization of light is mandatory for efficient harmonics generation in nonlinear optical crystals.

Resistance to photodarkening of the amplifier fiber is also of tremendous importance for harmonics generation as output power stability is essential for reliable system operation, especially for schemes based on successive conversion stages such as THG and further on in the deep UV. An accelerated test performed on a 50 cm-long fiber sample with average inversion of 38% has shown excess loss < 0.05 dB at 1064 nm after near 600 hours (see Fig. 1). The latter translates to photodarkening loss α_{PD} < 5 dB/m at 633 nm upon stabilization (and under full inversion), assuming a scaling factor of 30 between losses measured at 633 nm and 1064 nm [7]. The photodarkening losses reported herein compares favorably to data published about Yb-doped fibers sourced from other manufacturers. Besides, the fiber once configured as a laser amplifier has shown very minimal decline in output power during life tests spanning over 10^3 hours, except for spontaneous drops due to failures of individual emitters in pump laser diodes. Other properties of this fiber have already been discussed elsewhere [8].

2.2 NIR MOPA Laser

Pulse generation in the master oscillator is first initiated from direct current modulation of a wavelength-stabilized laser diode emitting at 1064 nm (see Fig. 2). In consequence, the pulse duration at the oscillator output could be kept constant regardless of the pulse repetition frequency (PRF). Synchronous phase modulation is then superimposed onto the nanosecond seed pulses using an EOM to lessen SBS in fiber amplifiers downstream. Linewidth broadening derived from phase modulation was limited to < 0.5 nm, not to exceed the spectral acceptance of nonlinear optical crystals used in latter SHG/THG stages. Subsequent amplifier chain consists of two successive pre-amplifier stages, the first one using

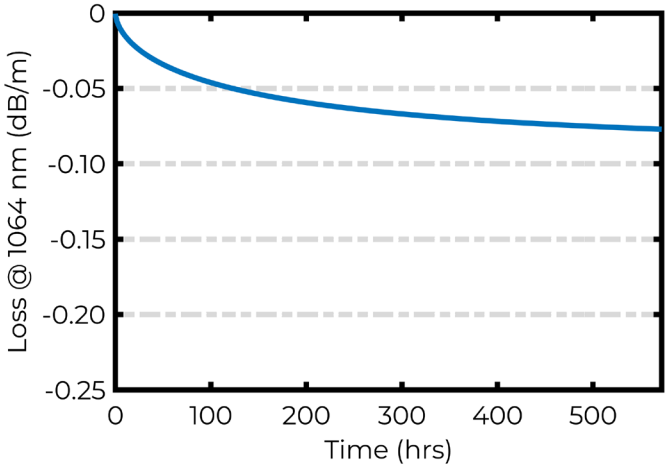

Figure 1 – Photodarkening loss α_{PD} at 1064 nm of the Yb-doped tapered fiber.

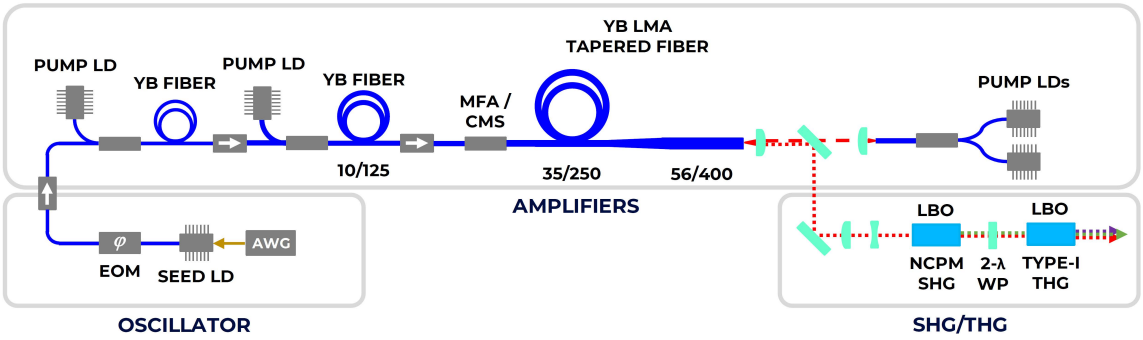

Figure 2 – Schematic representation of the experimental setup used for second- and third-harmonic generation (AWG: arbitrary waveform generation; LD: laser diode; EOM: electro-optic modulator; MFA: mode-field adapter; CMS: cladding mode stripper; LBO: LiB_3O_5 crystals; 2-λ WP: dual-wavelength wave plate).

single-mode single-clad fiber and the second one using double-clad fiber, along with the final amplifier stage, the latter taking advantage of the flared geometry of the tapered fiber, with core/cladding diameters of 56/400 µm at the large end. With a nominal pump absorption of 10 dB/m at 976 nm, the optimal fiber length was determined only slightly over 2 m. The amplifier fiber was actively cooled while the latter was fitted on a cold plate mount with recirculating liquid coolant for efficient dissipation of waste heat. The end cap spliced to the fiber distal end was sized so the laser peak fluence could be made low enough to avoid catastrophic damage on the AR-coated surface. Aspheric optics were used to launch the pump light at the same time as collecting signal light coming through this end of the amplifier fiber.

Counter pumping with 976-nm wavelength-stabilized laser diodes was shown to yield gain in the tapered fiber close to 30 dB, with output average power greater than 200 W and pulse energy exceeding 2 mJ, only limited by available pump power. Oscillator pulse repetition frequency of 200 kHz has served as a baseline for comparison purpose along this study (see Fig. 3), with PRF further being set in the range between 200-500 kHz for a few measurements. Out-of-band power due to amplified spontaneous emission (ASE) and stimulated Raman scattering (SRS) was seen to be negligible (see Fig. 3). Polarization extinction ratio was measured > 18 dB along the full operating range. In addition, near diffraction-limited output was achieved at the amplifier output with $M^2 \sim 1.2$ measured along horizontal/vertical axes (see Fig. 3). CCD blooming at 1064 nm is known to result in overestimation of D4σ widths measured by the beam propagation analyzer (acknowledged by the manufacturer); experience has shown that the actual M^2 are 0.05-0.10 smaller than the ones returned by the analyzer. Indeed, similar experiments have yield $M^2 < 1.1$ with laser wavelength set at 1036 nm [9], where blooming of CCD sensor is significantly less given the wavelength is further off from the silicon absorption edge.

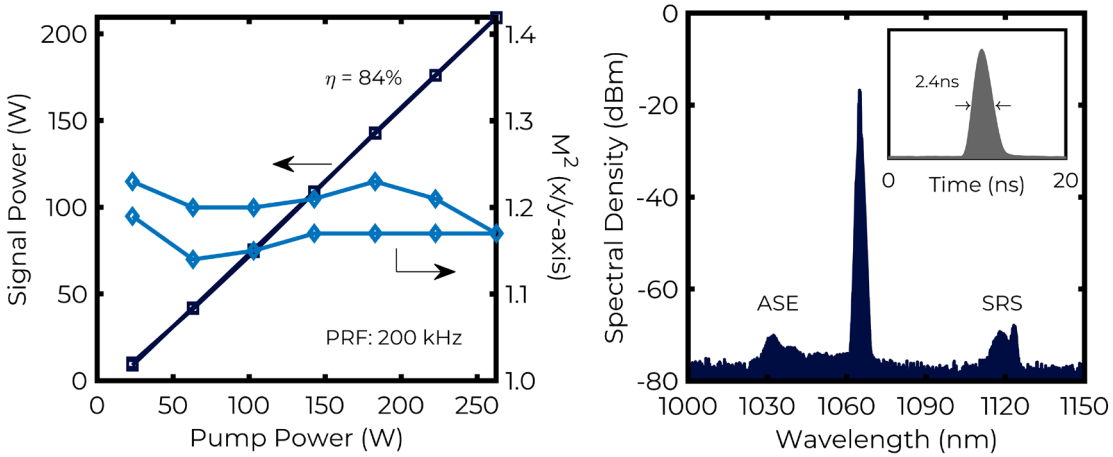

Figure 3 – NIR output power (with slope efficiency ~ 84 %) and beam quality (left); NIR spectrum corresponding to pulse energy of 1 mJ, duration of 2.4 ns (inset) and repetition frequency of 200 kHz (right).

Table 1 – Properties of nonlinear optical crystals used for SHG and THG (after [10]).

Mixing	Crystal	Size (mm^3)	T (°C)	θ, φ (deg)	ρ (deg)	$\Delta\lambda \cdot l$ (nm·cm)	$\Delta T \cdot l$ (°C·cm)
SHG	LBO-I	4x4x20	149	90, 0	–	3.73	5.3
THG	LBO-I	4x4x15	20	90, 37.2	1.05	0.75	18.7

3. HARMONICS GENERATION

UV generation was realized after single-pass SHG/THG using end-to-end LBO crystals (see Table 1). Second harmonic generation was first performed with a 20 mm-long type-I LBO crystal heated to 149 °C for non-critical phase matching. Third harmonic generation was next achieved through sum-frequency mixing of SHG and residual NIR using a 15 mm-long LBO crystal cut for type-I critical phase matching with proper angular adjustment. Properties listed in Table 1 for each wave-mixing process were obtained using recently-published Sellmeier dispersion relations for LBO crystals [10]. Type-I LBO was shown previously to yield better conversion efficiency because of its larger effective nonlinear coefficient and walk-off of THG product beam only [11]. Also type-I LBO has a much larger temperature acceptance which may help prevent thermally-induced phase mismatch due to crystal absorption at high average power and subsequent self-heating problem. Spectral acceptance of type-I mixing in LBO is however ~ 10% narrower than type-II mixing, which is nonetheless considered inconsequential given the larger effective nonlinear coefficient for type-I interaction and the fact that the output intensity of THG product beam is proportional to d_{eff}^2.

The NIR beam waist at the amplifier output was dimensioned to get decent efficiency after single-pass conversion through successive crystals and yet avoid excessive depletion regardless of oscillator pulse repetition frequency. A dual-wavelength wave plate with λ/2 retardation at 1064 nm and λ retardation at 532 nm was inserted between both crystals to have both SHG and residual NIR polarizations collinear for type-I mixing thereafter. Dichroic mirrors were used to separate harmonics from residual NIR after THG stage. Visible (532 nm) and UV (355 nm) average powers exceeding 100 W and 50 W were readily obtained after single-pass SHG/THG conversion scheme, with the latter being limited only by the NIR pump power (see Fig. 4). Besides, pulse energies for SHG and THG were seen to extend between 200-490 μJ and 105-260 μJ, respectively, with the oscillator pulse repetition frequency set in the range 200-500 kHz (see Fig. 4). Conversion efficiency from NIR to UV was found in the range 26-32 %, considering only the fraction of light lying within the spectral acceptance of THG crystal. Conversion efficiency did not seem to change much within the PRF range investigated, perhaps because SPM-induced spectral broadening is more significant at the lower bound of the oscillator pulse repetition frequency, with further energy shed beyond the spectral acceptance of THG nonlinear crystal.

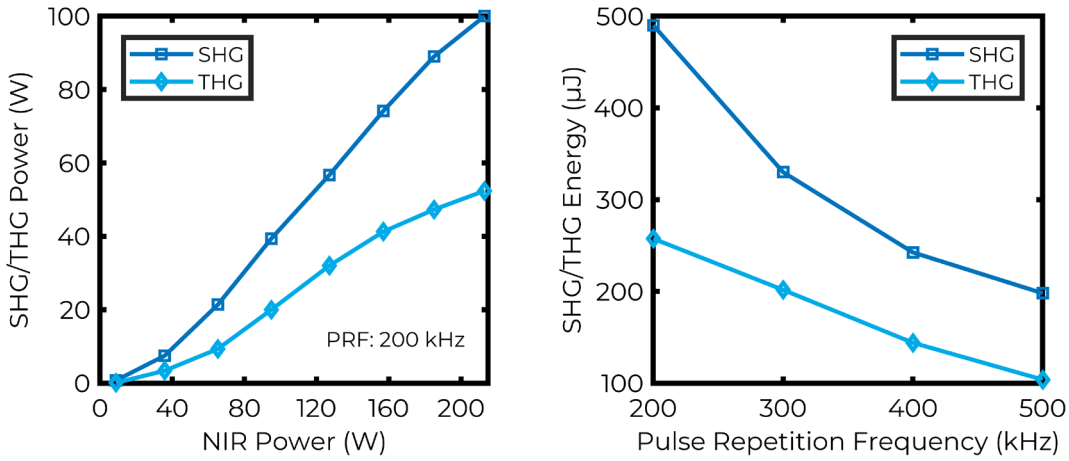

Figure 4 – Average power after SHG/THG as a function of NIR laser power with pulse repetition frequency of 200 kHz (left); pulse energy after SHG/THG with respect to pulse repetition frequency of NIR laser (right).

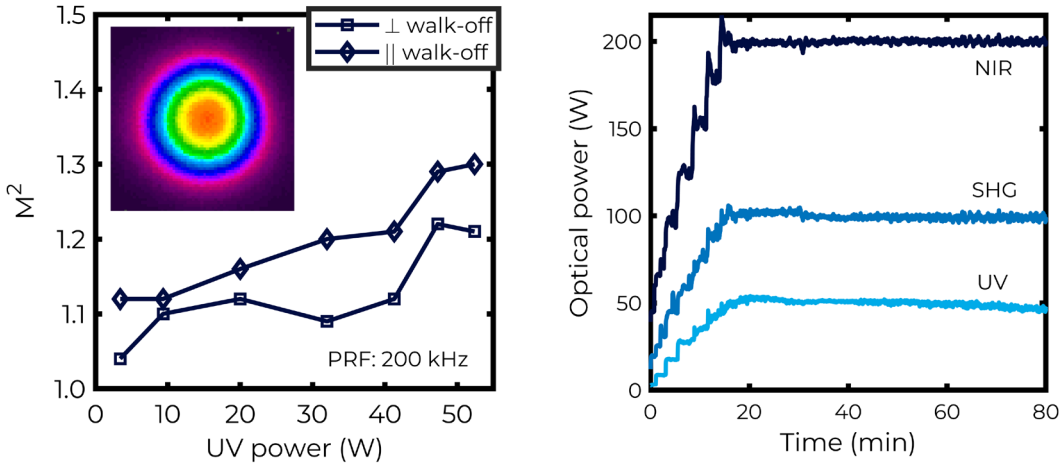

Figure 5 – UV beam quality M^2 with THG output average power (left) and UV beam profile (inset); NIR, SHG and UV output powers during a laser system life test.

Efficiency roll-off was observed at high power for both SHG and THG, with the latter more noticeable. Also, UV beam quality was seen to deviate from diffraction-limited output for increasing power, with M^2 factor extending from 1.1 to 1.3 both along and perpendicular to walk-off axis (see Fig. 5). Pulse lengthening was noticed with increasing output power after THG stage as well, with UV pulse duration ranging between 1.7-2.4 ns. While the latter picture is not inconsistent with depletion of NIR beam, all the above-mentioned observations were more pronounced than initially predicted by simulations. Bulk absorption in SHG/THG crystals and subsequent effect on conversion efficiency via the thermophysical properties of LBO were ignored from the model though. Nonetheless, despite the recent reports for nonlinear absorption in LBO and seemingly unfavorable type-I phase-matching in this respect [12-13], it is questionable whether the latter could explain the observations reported herein given that the laser peak intensity at the beam waist was relatively low (< 200 MW/cm^2). Indeed, solving the heat equation with absorption coefficients in [12] yields a temperature gradient ~ 1 °C in the crystal, i.e. much less than the temperature acceptance for type-I THG in LBO.

Besides, an hour-long life test has shown a slight drift in output power after THG stage (see Fig. 5). Visual inspection of THG crystal after several days of experiments did show some blemish on the AR coating crystal end face. Very superficial damage could further be observed using a 3D optical microscope, the latter revealing a damage extent less than 1μm deep, which incidentally corresponds to the thickness of AR coating dielectric layer stack. At this time, it is uncertain whether this damage was caused by excessive heat buildup through the dielectric coating layers, which likely would have the actual laser-induced damage threshold below the one provided by the manufacturer. Using a Brewster-cut crystal for instance would most likely solve this issue and have the system lifetime extended.

4. CONCLUSION

Tapered fibers have emerged as a truly scalable concept for high energy amplifiers in recent years, with reports of MW-mJ diffraction-limited outputs and now kW average powers [14]. The flared waveguide geometry is beneficial in many ways, first and foremost with the expanded mode area and increased nonlinear scattering threshold along the amplifier fiber, thus allowing for larger pulse peak powers. The latter, in turn, eases the design of the frequency conversion stage for harmonics generation in the UV, as decent efficiency can now be achieved under loose focusing and further with the output beam free of distortions due to walk-off. Ultimately, excellent beam quality and superior resistance to photodarkening of rare-earth-doped optical fibers such as the one described herein are pivotal to laser system reliability for scientific/industrial uses. The master-oscillator and power-amplifier system described herein, along with the frequency conversion stages delivering 100s μJ pulses in VIS and UV ranges, will no doubt prove advantageous for laser materials processing applications. Transparent and/or brittle materials such as ceramics and glasses are known to benefit from the use of short-wavelength lasers for scribing and cutting for example. It is further expected that the efficiency of fourth-harmonic generation would likewise scale to output powers beyond those available from commercial laser systems, provided the nonlinear crystal is conditioned to avoid UV-induced degradation.

REFERENCES

[1] Starodoumov, A. and Hodgson, N., "Harmonic generation with fiber MOPAs and solid state lasers: technical challenges, state-of-the-art comparison and future developments," in Solid-State Lasers XX: Technology and Devices, eds A. Clarkson, N. Hodgson and R. Shori, Proc. of SPIE 7912, 79120H (2011).

[2] Avdokhin, A., Gapontsev, V., Kadwani, P., Vaupel, A., Samartsev et al., "High average power quasi-CW single-mode green and UV fiber lasers," in Nonlinear Frequency Generation and Conversion: Materials, Devices and Applications XIV, ed K. L. Vodopyanov, Proc. of SPIE 9347, 934704 (2015).

[3] Saby, J., Cocquelin, B., Sangla, D. and Salin, F., "High power IR, green and UV fiber lasers," in Lasers, Sources, and Related Photonic Devices OSA Technical Digest, FTh5A.3 (2012).

[4] Tsubakimoto, K., Yoshida, H. and Miyanaga, N., "600 W green and 300 W UV light generated from an eight-beam, sub-nanosecond fiber laser system," Opt. Lett. 42(17), 3255-3258 (2017).

[5] Filippov, V., Chamorovskii, Y., Kerttula, J., Golant, K., Pessa, M. and Okhotnikov, O. G., "Double clad tapered fiber for high power applications," Opt. Express 16(3), 1929-1944 (2008).

[6] DiGiovanni, D. J. MacChesney, J. B. and Kometani, T. Y., "Structure and properties of silica containing aluminum and phosphorus near the $AlPO_4$ join," J. Non-Crystal. Solids 113(1), 58-64 (1989).

[7] Laperle, P., Desbiens, L., Le Foulgoc, K., Drolet, M., Deladurantaye, P. et al., "Modeling the photodegradation of large mode area Yb-doped fiber power amplifiers," in Fiber Lasers VI: Technology, Systems and Applications, eds D. V. Gapontsev, D. A. Kliner, J. W. Dawson and K. Tankala, Proc. of SPIE 7195, 71952C (2009).

[8] Roy, V., Paré, C., Labranche, B., Laperle, P., Desbiens, L. et al., "Yb-doped large mode area tapered fiber with depressed cladding and dopant confinement," in Fiber Lasers XIV: Technology, Systems and Applications, eds C. A. Robin and I. Hartl, Proc. of SPIE 10083, 1008314 (2017).

[9] Desbiens, L., Roy, V., Gravel, J. F. and Taillon, Y., "2.5 W, narrow linewidth, 259.0 nm, ruggedized DUV fiber laser source for remote benzene detection," CLEO/Europe-EQEC, Munich, Germany, pp. 1-1 (2019).

[10] Kato, K., Grechin, S. G. and Umemura, N., "New thermo-optic dispersion formula for LiB_3O_5," Laser Phys. 28, 095403 (2018).

[11] Gapontsev, V. P., Tyrtyshnyy, V. A., Vershinin, O. I., Davydov, B. L. and Oulianov, D. A., "Third harmonic frequency generation by Type-I critically phase-matched LiB_3O_5 crystal by means of optically active quartz crystal," Opt. Express 21, 3715-3720 (2013).

[12] Vershinin, O. I., Konyashkin, A. V. and Ryabushkin, O. A., "Anisotropy of nonlinear optical absorption of LBO crystals at 355 nm," Opt. Lett. 43, 58-61 (2018).

[13] Mühlig, C. and Bublitz, S., "Characterization of nonlinear optical crystal absorption," Opt. Engineering 57, 121907 (2018).

[14] Ye, Y., Xi, X., Shi, C., Yang, B., Wang, X. et al, "Comparative study on transverse mode instability of fiber amplifiers based on long tapered fiber and conventional uniform fiber," Laser Phys. Lett. 16(8), 085109 (2019).